JMEPEG (2012) 21:2238–2243
DOI: 10.1007/s11665-012-0172-9

1059-9495/$19.00

Modeling the Flow Curve of AISI 410 Martensitic Stainless Steel

A. Momeni, K. Dehghani, M. Heidari, and M. Vaseghi

(Submitted July 19, 2011; in revised form January 28, 2012)

In the present study, hot deformation behavior of AISI 410 martensitic stainless steel was investigated and modeled after conducting compression tests at the temperature range of 900-1150 °C and strain rate range of 0.001-1 s^{-1}. At the studied temperature and strain rates, the flow curves were typical of dynamic recrystallization (DRX) showing a hardening peak followed by a softening one, and a steady state. The flow curves up to the peaks were modeled using the Estrin and Mecking equation. The softening due to DRX was also considered to increase the consistency of the developed model. The experimental equation proposed by Cingara and McQueen was also used to model the work hardening region. The results showed that the phenomenological model based on the Estrin and Mecking equation resulted in a better model for the work hardening region. Based on the Avrami equation, a model was developed to estimate the flow softening due to DRX between the peak and the starting point of steady state. The average value of the Avrami exponent was determined as 2.2, and it decreased with the increasing Zener-Hollomon parameter.

Keywords constitutive equation, dynamic recrystallization, flow curve, hot deformation

1. Introduction

Martensitic stainless steels are among the most widely used materials because of their high strength and good corrosion resistance. Among the martensitic stainless steels, AISI 410 is a well-known grade which is widely used for different applications, such as valves, shafts, and bearings, where high strength, high toughness, and good corrosion resistance are required (Ref 1). The martensitic stainless steels are widely used as semi-finished or near-net shaped products by taking the advantage of controlled hot working operations. Creating the desired shape and refining the austenite phase at high temperatures before transforming the structure to martensite are the main concerns during the hot deformation process of these steels. This is known as the "high-temperature thermomechanical treatment" (HTMT). The HTMT is defined based on the fact that the finer the austenite grain is, the finer the structure of martensite will be (Ref 2). Thus, a proper HTMT not only modifies the microstructure but also inhibits the precipitation of undesirable phases. The HTMT process is often applied through industrial hot forging of these steels.

Dynamic recrystallization (DRX) is known to be the dominant restoration mechanism regarding the hot deformation of stainless steels. The austenite structure is significantly refined via DRX resulting in the improvements of final mechanical properties (Ref 3-7). During hot deformation, DRX occurs after the accumulated stored energy reaches a critical value (Ref 8). Following work hardening, DRX commences and results in a gradual decrease in the flow stress. The initial work hardening followed by softening through DRX leaves a peak on the flow curve. Although the peak in the flow curve is commonly assumed as the onset of restoration process, DRX actually starts at a critical strain (ε_c) which is about 0.8 times the peak strain (ε_p) value (Ref 9). Following the peak, there is an increase in the work-softening rate followed by a drop in the softening rate until a steady state, which is the balance between DRX and the concurrent hot work hardening, is attained (Ref 9).

Many of the previous investigations have been devoted to model the flow curve (Ref 10-13). However, different microstructural phenomena occurring before and after the peak stress/strain have necessitated the researchers to use different models. For example, before the peak, the increase in dislocation density due to work hardening and the dislocation annihilation and rearrangement because of dynamic recovery (DRV) are the competing phenomena. The overall effects of these counteracting phenomena on the flow curve and the peak stress/strain are modeled based on the Estrin and Mecking formulation as well as the Cingara–McQueen empirical equation (Ref 12, 14). The concern regarding these models is that they cannot describe the interaction that exists between the initial DRV and the subsequent DRX. Beyond the peak, DRX takes place as the dominant restoration mechanism via nucleation and growth (Ref 15, 16). Therefore, its kinetics is often modeled by the Avrami equation. Although there are many investigations trying to model the DRX flow curve (Ref 10, 17, 18), their applicability has been limited for some simplifying assumptions. Therefore, the present investigation was devoted to evaluate the applicability of empirical and phenomenological formulations to model the typical flow curves in AISI 410 stainless steel.

2. Experimental Procedures

The material used in this investigation was 410 martensitic stainless steel grade having the composition of Fe +

A. Momeni and **M. Vaseghi**, Materials Science and Engineering Department, Hamedan University of Technology, Hamedan, Iran; and **K. Dehghani** and **M. Heidari**, Department of Mining and Metallurgy, Amirkabir University of Technology, Tehran, Iran. Contact e-mail: ammomeni@ aut.ac.ir.

0.06C + 13.00Cr + 0.8Si + 1.00Mn + 0.03S (in wt.%). Cylindrical compression samples of 10-mm height and 15-mm diameter were prepared from the as-received hot-forged bar. Concentric grooves of 0.5-mm depth were machined on the surfaces of compression samples to keep the lubricant (graphite) between the contacting surfaces. The temperature of the specimens was monitored using a chromel-alumel thermocouple embedded in the mid-height of the samples. The temperatures were also checked with the outer indicator of the heating furnace. An Instron 8502 testing machine, equipped with a fully computerized furnace, was used to perform the hot compression tests. Before testing, all the specimens were heated to 1200 °C, soaked for 15 min, and then cooled down at 15 °C/min. to the testing temperature. Continuous hot compression tests were carried out at temperatures of 900-1150 °C with the intervals of 50 °C and at strain rates ranging from 10^{-3} to 1 s^{-1}.

3. Results and Discussion

3.1 The Hot Deformation Behavior

Figure 1 shows the flow curves obtained at the investigated hot compression conditions. As expected, for a given deformation temperature, the flow-stress level increases with strain rate. Also, the typical form of DRX flow curve is observed at high temperatures and low strain rates. At high strain rates, concurrent deformation decelerates the rate of work softening. Consequently, the peak point and the steady-state flow, known as the characteristic points of a typical flow curve, are shifted to higher strain levels. It is also evident that the higher the deformation temperature is, the lower the flow-stress level and the characteristic strains, i.e., the peak and steady-state strains, will be. Although most flow curves indicate a single peak, the multi-peak behavior is often observed at low strain rates and high temperatures. In case of multi-peak behavior, the successive DRX cycles are completed before the next one starts. By contrast, in single-peak case, the successive cycles of nucleation overlap so that a single-peak curve appears (Ref 19). It is important to note that the multi-peak flow curves is not simply modeled using the existing phenomenological or experimental models and most of models are applied to the single-peak behavior which is more common during hot deformation.

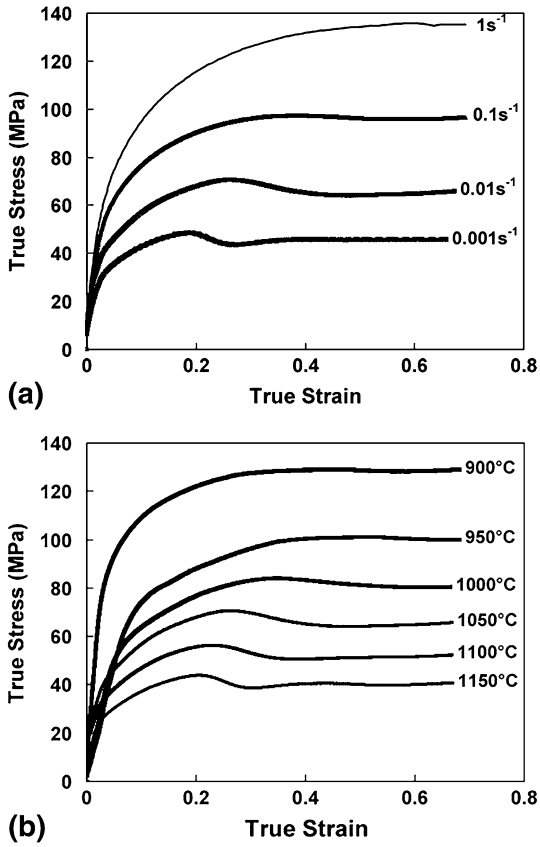

Fig. 1 Typical flow curves obtained at different deformation conditions: (a) 1050 °C and (b) 0.01 s^{-1}

3.2 Modeling the Work Hardening Region

3.2.1 Dislocation Density Evolution Modeling and Flow Equation According to the DRV Equation. In the first region of hot-deformation curve, work hardening and DRV occur concomitantly. However, in the low SFE materials, such as austenitic steels, the micromechanisms of DRV, i.e., dislocation annihilation and rearrangement, occur sluggishly. This gives rise to the build-up of dislocation density until reaching the critical strain (ε_c) required for DRX. This scenario pushed the previous scientists to use different evolution functions describing the variation of dislocation density during work hardening and DRV. These approaches finally aimed at the formulation of the flow curve. In an evolution function, the change in the dislocation density during hot working can be assumed as the sum of differential hardening and softening terms, given by

$$\frac{d\rho}{d\varepsilon} = \left(\frac{d\rho}{d\varepsilon}\right)^{+} + \left(\frac{d\rho}{d\varepsilon}\right)^{-} \quad \text{(Eq 1)}$$

On the right-hand side of Eq 1, the first term stands for work hardening part, and the second term denotes the contribution of DRV. In the present study, the dependence of the dislocation density on plastic strain is expressed by the equation proposed by Estrin and Mecking (Ref 14):

$$\frac{d\rho}{d\varepsilon} = h - r\rho \quad \text{(Eq 2)}$$

where h is the athermal work-hardening rate, and r denotes the rate of dynamic recovery at a given temperature and strain rate. Both h and r are considered independent of the applied strain. The above differential equation gives the following descriptions of dislocation density and flow stress as a function of plastic strain:

$$\rho = \left(\frac{h}{r}\right) - \left(\frac{h}{r} - \rho_0\right)\exp(-r\varepsilon) \quad \text{(Eq 3)}$$

$$\sigma = \left[\sigma_{rec}^2 - \left(\sigma_{rec}^2 - \sigma_0^2\right)\exp(r\varepsilon)\right]^{0.5} \quad \text{(Eq 4)}$$

where σ_0 and σ_{rec} refer to the initial and saturated stress defined as $(\alpha MGb)\rho_0^{0.5}$ and $(\alpha MGb)(h/r)^{0.5}$, respectively. The parameter α is a shape factor in the order of unity, M is the Taylor factor (3.07 for FCC materials), G is the shear modulus, b is the magnitude of Burger's vector, and ρ_0 is the initial dislocation density. It is notable that irrespective of the mechanical processes within the sample, flow stress is determined using the dislocation density as $(\alpha MGb)\rho^{0.5}$. Referring

to the flow curves presented in Fig. 1, the work-hardening rate at the early stages of deformation is high enough to justify the simplified assumption that ρ_0 is almost negligible on comparing to the generated dislocation density during hot deformation. This assumption is also more applicable to low SFE materials such as austenitic steels characterized by a sluggish DRV process. Therefore, by neglecting ρ_0 and σ_0, the simplified descriptions of the dislocation density and flow stress can be considered as follows:

$$\rho = \left(\frac{h}{r}\right)(1 - \exp(-r\varepsilon)) \quad \text{(Eq 5)}$$

$$\sigma = \sigma_{rec}(1 - \exp(-r\varepsilon))^{0.5} \quad \text{(Eq 6)}$$

Equation 6 can be used to determine the values of σ_{rec} and r in a way described by the authors elsewhere (Ref 20). The formalism of $\sigma(\varepsilon)$ developed in Eq 6 actually describes the flow curve when DRV is dominant. It is generally accepted that the rate of DRV decreases as strain rate rises or temperature declines. This fact implies the dependence of σ_{rec} and r on the deformation condition generally described by the Zener-Hollomon parameter. The following equations were proposed according to the previous articles (Ref 20, 21):

$$Z = \dot{\varepsilon}\exp\left(\frac{448000}{8.314T}\right) \quad \text{(Eq 7)}$$

$$r = 454.9Z^{-0.11} \quad \text{(Eq 8)}$$

$$\sigma_{rec} = 0.3Z^{0.15} \quad \text{(Eq 9)}$$

As indicated by some typically calculated flow curves in Fig. 2, Eq 6-9 can be used to predict the work-hardening region of the flow curve at different deformation conditions.

3.2.2 Law of Mixture. As mentioned, the concept of the formulation with Eq 6-9, is based on the work hardening and DRV, and therefore it is applicable up to the critical point at which DRX starts. It is evident that the predicted flow curves deviate from the experimental ones at a point beyond the peak, which is generally known as the critical point of DRX. In the strain range between critical and peak points, the softening due to DRX causes the experimental curve to deviate from the predicted one.

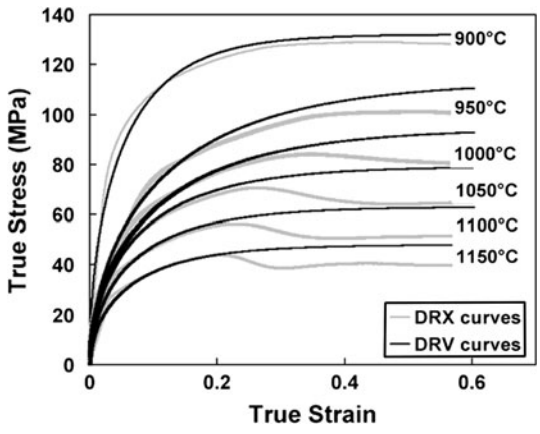

Fig. 2 Measured flow curves (gray lines) and modeled flow curves according to Eq 6-9 (black lines). The modeling holds only up to the critical strain, and plotting beyond that point serves to illustrate the domination of DRX afterward

In order to model this part of the flow curve, the first step is to determine the critical point as a function of deformation variables. According to the method developed by Poliak and Jonas (Ref 22, 23), the onset of DRX can be identified as the inflection point of the θ-σ curve (θ is the work-hardening rate) near the peak stress. The observed inflection in the θ-σ curves is associated with the softening because of the first bulges appearing at the early stages of DRX. In this method, the peak strain is also identified at $\theta = 0$. Momeni et al. (Ref 20) used this method and indicated the dependences of critical and peak strains, ε_c and $\varepsilon_{p,}$, respectively, and the peak stress, σ_p upon the Z parameter:

$$\varepsilon_c = 0.007Z^{0.09} \quad \text{(Eq 10)}$$

$$\varepsilon_p = 0.003Z^{0.12} \quad \text{(Eq 11)}$$

$$\sigma_p = 0.27Z^{0.15} \quad \text{(Eq 12)}$$

The authors further showed that the fraction affected by DRX softening (X_{DRX}) increases from 0% at the critical strain (ε_c) to about 10% at the peak strain (ε_p) (Ref 20). Even though X_{DRX} values fit over a sigmoidal curve with increasing strain, the proximities of ε_c and ε_p ($\varepsilon_c \sim 0.8\ \varepsilon_p$) allow the X_{DRX} to be linearly fitted to strain as follows:

$$X_{DRX} = 0.1\left(\frac{\varepsilon - \varepsilon_c}{\varepsilon_p - \varepsilon_c}\right) \quad \text{(Eq 13)}$$

At strains higher than ε_c, microstructure is actually duplex. One part experiences DRX resulting in a decreasing dislocation density, while the other part undergoes DRV leading to higher dislocation density. Therefore, from the law of mixture, the flow stress can be defined as follows:

$$\sigma = X_{DRX} \cdot \sigma_{DRX} + (1 - X_{DRX}) \cdot \sigma_{DRV} \quad \text{(Eq 14)}$$

where σ_{DRX} and σ_{DRV} are the respective flow stress terms of DRX and DRV according to the dominating mechanisms, DRV and DRX, respectively. Equation 14 can be rewritten as follows:

$$\sigma = \alpha MGb\left[X_{DRX} \cdot \rho_{DRX}^{0.5} + (1 - X_{DRX}) \cdot \rho_{DRV}^{0.5}\right] \quad \text{(Eq 15)}$$

Combining Eq 5 and 15 and considering $\sigma = (\alpha MGb)\rho^{0.5}$ yield the following description of flow stress in the strain region between ε_c and ε_p:

$$\sigma = \alpha MGb\left(\frac{h}{r}\right)^{0.5}\left[X_{DRX} \cdot \{1 - \exp(-r(\varepsilon - \varepsilon_c)\}^{0.5} + (1 - X_{DRX}) \cdot \{1 - \exp(-r\varepsilon)\}^{0.5}\right] \quad (Eq16)$$

The flow curves simulated according to Eq 16 are shown in Fig. 3. The values reported in the literature were replaced for α, M, b, and G (Ref 20). From Eq 8 and 9 and considering $\sigma_{rec} = (\alpha MGb)(h/r)^{0.5}$, h can be determined as follows:

$$h = \left(\frac{6.4}{\alpha MGb}\right)^2 Z^{0.19} \quad \text{(Eq 17)}$$

Figure 3 indicates that Eq 16, which takes into account the softening due to DRX, gives a good approximation of flow curve between the critical and peak points. The results of this equation are slightly better than those of DRV formulation at low temperatures where DRV is inherently sluggish.

3.2.3 Cingara and McQueen Modeling. To model the flow curve up to the peak point, the empirical equation proposed by Cingara and McQueen (Ref 12) can be used instead of the phenomenological approaches addressed in the previous section. It is given as follows:

$$\frac{\sigma}{\sigma_p} = \left[(\varepsilon/\varepsilon_p)\exp(1-\varepsilon/\varepsilon_p)\right]^c \quad \text{(Eq 18)}$$

where, c is a constant determined experimentally. The experimental data on a logarithmic scale plot can be used to determine the value of c. The plot of $\ln(\sigma/\sigma_p)$ vs. $1-\varepsilon/\varepsilon_p + \ln(\varepsilon/\varepsilon_p)$ shown in Fig. 4 was used, and the average value of c was found to be 0.47. This is higher than the value of 0.2 reported by Cingara and McQueen (Ref 12) for 300 series stainless steels. The difference may be due to the different work-hardening rates and DRV behaviors of the alloys. The c value actually determines the speed at which stress increases with strain, the so-called work-hardening rate. In other words, the lower the c value is, the lower the work-hardening rate or the higher the rate of DRV will be. This is consistent with the lower alloying content of the studied steel compared with high alloy AISI 300 series stainless steels.

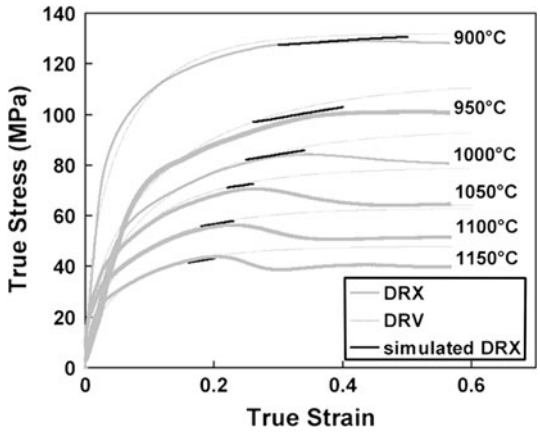

Fig. 3 Simulated flow curves superimposed with short black lines to model the interval between the critical point and the peak point (Eq 16)

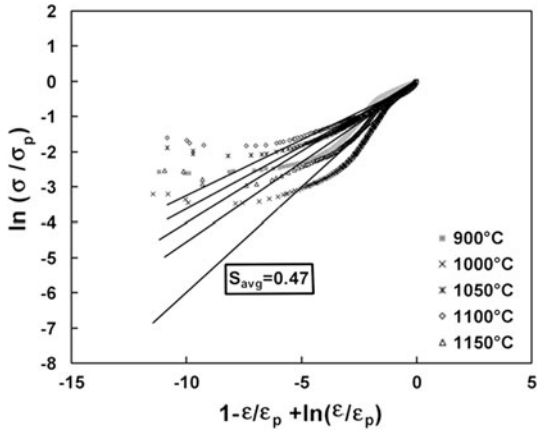

Fig. 4 Plots of flow data according to the Cingara–McQueen equation. The plots are drawn at a constant strain rate of 0.01 s^{-1} and different temperatures

The value of c was found nearly independent on strain rate and actually decreased with temperature. The strong dependence of c on temperature clearly confirms its relation with the rate of DRV. It implies the fact that at higher temperatures, DRV is more efficient and decelerates the work-hardening rate. Using the average value of c obtained here and combining Eq 11, 12 and 18, an experimentally based formalism can be proposed to model a typical DRX flow curve up to the peak:

$$\sigma = 4.14\varepsilon^{0.47}Z^{0.094}\exp\left(0.47 - 156.67\varepsilon Z^{-0.12}\right) \quad \text{(Eq 19)}$$

The predicted flow curves shown in Fig. 5 indicate that the phenomenological models proposed in Eq 6 and 16 give a better approximation of the flow curve up to the peak.

3.3 Modeling the DRX Softening

Because of different microstructural phenomena dominated at different regions of a typical flow curve, it is very difficult to propose a comprehensive model covering all these regions. For instance, after the peak, the DRX occurs because of the nucleation and the growth of new grains. A modified form of the Avrami equation has been developed to model the kinetics of DRX as a function of strain as follows (Ref 19):

$$X = 1 - \exp[-\xi(\varepsilon - \varepsilon_c)^{\eta}] \quad \text{(Eq 20)}$$

where X denotes the fraction affected by softening, and ξ and η are the material constants. In order to use this kinetics equation as a way to model the softening due to DRX, a simplified form of Eq 17 has been used in the literature (Ref 11). Equation 20 can be written as follows (Ref 24):

$$X = 1 - \exp\left(-0.693\left(\frac{\varepsilon - \varepsilon_c}{\varepsilon^*}\right)^n\right) \quad \text{(Eq 21)}$$

where ε^* stands for the strain at which DRX provides the highest rate of softening and is equal to $\varepsilon_{0.5} = (\varepsilon_p + \varepsilon_s)/2$, where ε_s is the strain at the beginning of steady-state region. The actual softening due to DRX can be considered as corresponding to the decrease in flow stress from σ_p to σ_s. Assuming $X = 0.1$ at the peak strain (referring to Eq 13) according to the literature (Ref 20), the fractional softening can be written as follows:

$$X = X|_{\varepsilon_c}^{\varepsilon_p} + X|_{\varepsilon_p}^{\varepsilon_s} \quad \text{(Eq 22)}$$

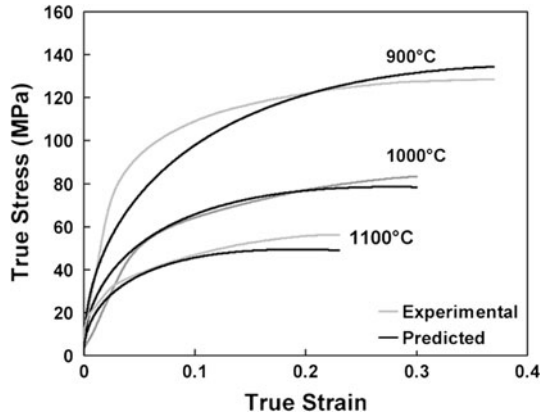

Fig. 5 Prediction of flow curves using the Eq 18 at a constant strain rate of 0.01 s^{-1}

$$X|_{\varepsilon_p}^{\varepsilon_s} = \frac{\sigma_p - \sigma}{\sigma_p - \sigma_s} \quad \text{(Eq 23)}$$

Finally, the modified form of the Avrami equation for DRX is derived as

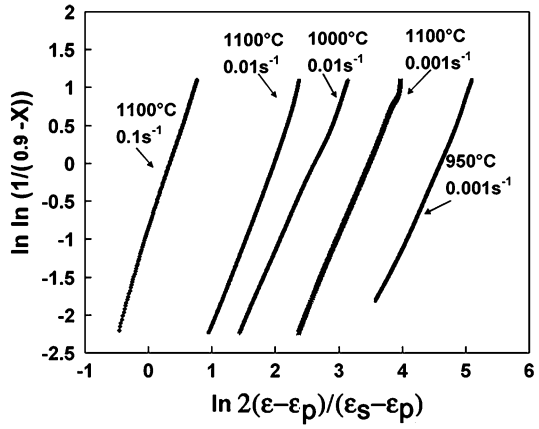

Fig. 6 The Avrami plots for the determination of n at different deformation conditions

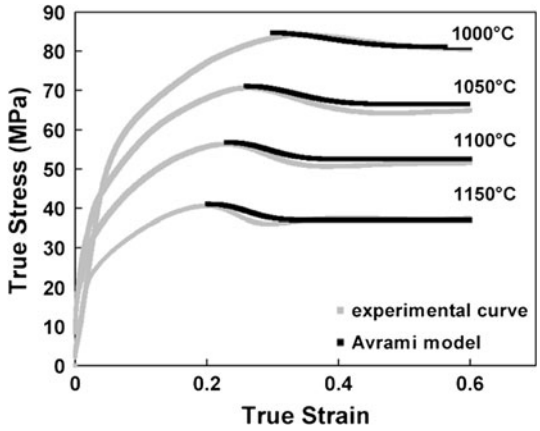

Fig. 7 DRX flow softening modeled using the Avrami equation at constant strain rate of 0.01 s^{-1}

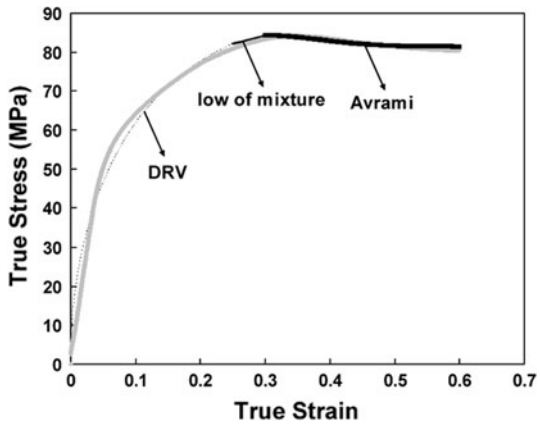

Fig. 8 The flow curve at a temperature of 1000 °C and a strain rate of 0.01 s^{-1} model by a combination of DRV approach, law of mixture, and Avrami equation

$$X|_{\varepsilon_p}^{\varepsilon_s} = \frac{\sigma_p - \sigma}{\sigma_p - \sigma_s} = 0.9 - \exp\left[-0.693\left(\frac{2(\varepsilon - \varepsilon_p)}{\varepsilon_s - \varepsilon_p}\right)^n\right] \quad \text{(Eq 24)}$$

The exponent of n is determined by plotting $\ln(\ln(1/(0.9 - X))$ vs. $\ln\left(\frac{2(\varepsilon-\varepsilon_p)}{\varepsilon_s-\varepsilon_p}\right)$. Figure 6 shows the typical Avrami curves at different deformation conditions. Although n was found dependent on the deformation condition, its average value of 2.2 is in a good agreement with the value of 2 reported for DRX in the literature (Ref 19). Previous study conducted on the same alloy (Ref 11) has illustrated that n actually decreases with Z as follows:

$$n = 24.44Z^{-0.068} \quad \text{(Eq 25)}$$

As the rate at which X approaches unity depends on n, a higher temperature or lower strain rate results in a higher work-softening rate and lower n value. In order to utilize Eq 24 for modeling DRX flow curve, ε_s and σ_s were determined at different deformation conditions and correlated to Z as follows:

$$\varepsilon_s = 0.015Z^{0.093} \quad \text{(Eq 26)}$$

$$\sigma_s = 0.215Z^{0.157} \quad \text{(Eq 27)}$$

Figure 7 exhibits the predictions based of the Avrami kinetics equation at different deformation temperatures. Figure 8 combines the DRV approach, law of mixture, and the Avrami's equation to model the DRX flow curve at a temperature of 1000 °C and a strain rate of 0.01 s^{-1}. It is observed that the combination of these different approaches taken for different regions of flow curve results in a good approximation of practical behavior.

4. Conclusions

The flow curves of AISI 410 martensitic stainless steel at high temperatures were analyzed and modeled using different constitutive equations. The most important results are as follows:

1. At a wide temperature and strain-rate range, the flow curves of the studied alloy are typical of DRX showing work hardening to a peak, followed by flow softening and a plateau or steady state during hot deformation.
2. The work-hardening region up to the peak was modeled using the DRV method and also by considering the softening due to DRX after the critical strain. The developed method based on the law of mixture modeled the flow curve better than the DRV method.
3. The experimental equation proposed by Cingara and McQueen was also used to model the work-hardening region. The range of applicability of this equation was enlarged by taking into account the dependences of peak stress and strain on the Zenner-Hollomon parameter.
4. A model was also developed based on the Avrami equation to describe the flow curve from peak up to the maximum strain achieved. The average value of Avrami exponent was determined as 2.2, and it decreased with increasing Z parameter.

References

1. M.C. Tsai, C.S. Chiou, J.S. Du, and J.R. Yang, Phase Transformation in AISI, 410 Stainless Steel, *Mater. Sci. Eng.*, 2002, **A332**, p 1–10

2. C. Wang, M. Wang, J. Shi, W. Hui, and H. Dong, Effect of Microstructure Refinement on the Strength and Toughness of Low Alloy Martensitic Steel, *J. Mater. Sci. Technol.*, 2007, **23**, p 659–664
3. S. Venugopal, S.L. Mannan, and P. Rodriguez, Strategy for the Design of Thermomechanical Processes for AISI, type 304L Stainless Steel Using Dynamic Materials Model (DMM) Stability Criteria and Model for the Evolution of Microstructure, *J. Mater. Sci.*, 2004, **39**, p 5557–5560
4. A. Momeni, A. Shokuhfar, and S.M. Abbasi, Dynamic Recrystallization of a Cr-Ni-Mo-Cu-Ti-V Precipitation Hardenable Stainless Steel, *J. Mater. Sci. Technol.*, 2007, **23**, p 775–778
5. A. Dehghan-Manshadi, M.R. Barnett, and P.D. Hodgson, Recrystallization in AISI, 304 Austenitic Stainless Steel During and After Hot Deformation, *Mater. Sci. Eng. A*, 2008, **485**(1–2), p 664–672
6. A. Momeni, S.M. Abbasi, and A. Shokuhfar, Dynamic and Metadynamic Recrystallization of a Martensitic Precipitation Hardenable Stainless Steel, *Metal. Quart.*, 2007, **4**, p 189–193
7. A. Momeni and K. Dehghani, Prediction of Dynamic Recrystallization Kinetics and Grain Size for 410 Martensitic Stainless Steel During Hot Deformation, *Met. Mater. Int.*, 2010, **16**, p 843–849
8. R. Ding and Z.X. Guo, Coupled Quantitative Simulation of Microstructural Evolution and Plastic Flow During Dynamic Recrystallization, *Acta. Mater.*, 2001, **49**, p 3163–3175
9. S.H. Cho and Y.C. Yoo, Hot Rolling Simulation of Austenitic Stainless Steel, *J. Mater. Sci.*, 2001, **36**, p 4267–4272
10. J.J. Jonas, X. Quelennec, L. Jiang, and E. Martin, The Avrami Kinetics of Dynamic Recrystallization, *Acta Mater.*, 2009, **57**, p 2748–2756
11. A. Momeni, K. Dehghani, G.R. Ebrahimi, and H. Keshmiri, Prediction of Dynamic Recrystallization Kinetics and Grain Size for 410 Martensitic Stainless Steel During Hot Deformation, *Met. Mater. Trans.*, 2010, **41A**, p 2898–2904
12. A. Cingara and H.J. McQueen, New Method for Determining Sinh Constitutive Constants for High Temperature Deformation of 300 Austenitic Steels, *J. Mater. Process. Technol*, 1992, **36**, p 17–30
13. S. Serajzadeh, Thermo-Mechanical Modeling of Hot Forging Process, *J. Eng. Mater. Technol.*, 2004, **126**, p 406–412
14. Y. Estrin and H. Mecking, A Unified Phenomenological Description of Work Hardening and Creep Based on One-Parameter Models, *Acta Metall.*, 1984, **32**, p 57–70
15. X. Wang, E. Brunger, and G. Gottstein, Microstructure Characterization and Dynamic Recrystallization in an Alloy 800h, *Mater. Sci. Eng.*, 2000, **A290**, p 180–185
16. S. Mandal, P.V. Sivaprasad, and R.K. Dube, Kinetics, Mechanism and Modelling of Microstructural Evolution During Thermomechanical Processing of a 15Cr-15Ni-2.2Mo-Ti Modified Austenitic Stainless Steel, *J. Mater. Sci.*, 2007, **42**, p 2724–2734
17. A.M.J. Junior and O. Balancin, Prediction of Steel Flow Stresses Under Hot Working Conditions, *Mater. Res.*, 2005, **8**, p 309–315
18. H. Mirzadeh and A. Najafizadeh, Extrapolation of Flow Curves at Hot Working Conditions, *Mater. Sci. Eng.*, 2010, **A527**, p 1160–1164
19. W. Roberts, *Dynamic Changes that Occur During Hot Working and Their Significance Regarding Microstructural Development and Hot Workability*, G. Krauss, Ed., 1982 ASM Materials Science Seminar (St Louis, Missouri, OH, USA), ASM, 1982, p 109–184
20. A. Momeni, K. Dehghani, and G.R. Ebrahimi, Modeling the Initiation of Dynamic Recrystallization Using a Dynamic Recovery Model, *J. Alloys Compd.*, 2011, **509**, p 9387–9393
21. A. Momeni and K. Dehghani, Characterization of Hot Deformation Behavior of 410 Martensitic Stainless Steel Using Constitutive Equations and Processing Maps, *Mater. Sci. Eng.*, 2010, **A527**, p 5467–5473
22. E.I. Poliak and J.J. Jonas, Initiation of Dynamic Recrystallization in Constant Strain Rate Hot Deformation, *ISIJ Int.*, 2003, **43**, p 684–691
23. E.I. Poliak and J.J. Jonas, Critical Strain for Dynamic Recrystallization in Variable Strain Rate Hot Deformation, *ISIJ Int.*, 2003, **43**, p 692–700
24. G.E. Dieter, H.A. Kuhn, and S.L. Semiatin, *Handbook of Workability and Process Design*, ASM, Materials Park, OH, 2003, p 35–44